Refining Marine Net Primary Production Estimates: Advanced Uncertainty Quantification through Probability Prediction Models

Jie Niu[1,2†], Mengyu Xie[3†], Yanqun Lu[3*], Liwei Sun[4], Na Liu[5], Han Qiu[6], Dongdong Liu[1,2], Chuanhao Wu[7], Pan Wu[1,2*]

[1]College of Resources and Environmental Engineering, Guizhou University, Guiyang 550025, China

[2]Key Laboratory of Karst Georesources and Environment, Ministry of Education, Guiyang 550025, China

[3] Institute for Environmental and Climate Research, Jinan University, Guangzhou 510632, China

[4]Southern Marine Science and Engineering Guangdong Laboratory (Guangzhou), Guangzhou 511458, China

[5]College of Life Science and Technology, Jinan University, Guangzhou 510632, China

[6]Department of Sustainable Earth Systems Sciences, University of Texas, Dallas, Richardson, TX 75080, USA

[7]Yangtze Institute for Conservation and Development, Hohai University, Nanjing 210024, China

*Corresponding author: Yanqun Lu, Pan Wu

E-mail address: ~~Yanqunlv@163.com~~Yanqunlv@163.com, ~~pwu@gzu.edu.cn~~pwu@gzu.edu.cn

[†] These authors contributed equally to this work and should be considered co-first authors.

Abstract

In marine ecosystems, Net Primary Production (NPP) is important, not merely as a critical indicator of ecosystem health, but also as an essential component in the global carbon cycling process. Despite its significance, the accurate estimation of NPP is plagued by uncertainty stemming from multiple sources, including measurement challenges in the field, errors in satellite-based inversion methods, and inherent variability in ecosystem dynamics. This study focuses on the aquatic environs of Weizhou Island, located off the coast of Guangxi, China, and introduces an advanced probability prediction model aimed at improving NPP estimation accuracy while addressing partially its associated uncertainties within the current modeling framework. The dataset comprises eight distinct sets of monitoring data spanning from January 2007 to February 2018. NPP values were derived using three widely recognized

estimation methods — VGPM, CAFE, and CbPM — serving as model outputs for further analysis. The study evaluates two probability prediction approaches: a Bayesian probability prediction model based on empirical distribution and a deep learning-based probability prediction model. These methods are employed to meticulously quantify the uncertainty of NPP. The results highlight the effectiveness of probability prediction models in capturing the dynamic trends and uncertainties of marine NPP. Notably, the neural network-based model demonstrates superior accuracy and reliability compared to the Bayesian approach. Furthermore, the models are applied to prognosticate NPP variations in specific marine regions, efficaciously elucidating interannual trends. This research advances ~~both~~ the methodological precision in partially quantifying NPP uncertainty related to parameter and ~~provides robust scientific evidence~~input data variability, while highlighting the need for ~~marine ecosystems management and environmental conservation~~future structural uncertainty assessments through multi-model comparisons.

Keywords: Net Primary Production; Bayesian Probability Prediction; Neural Network Probability Prediction.
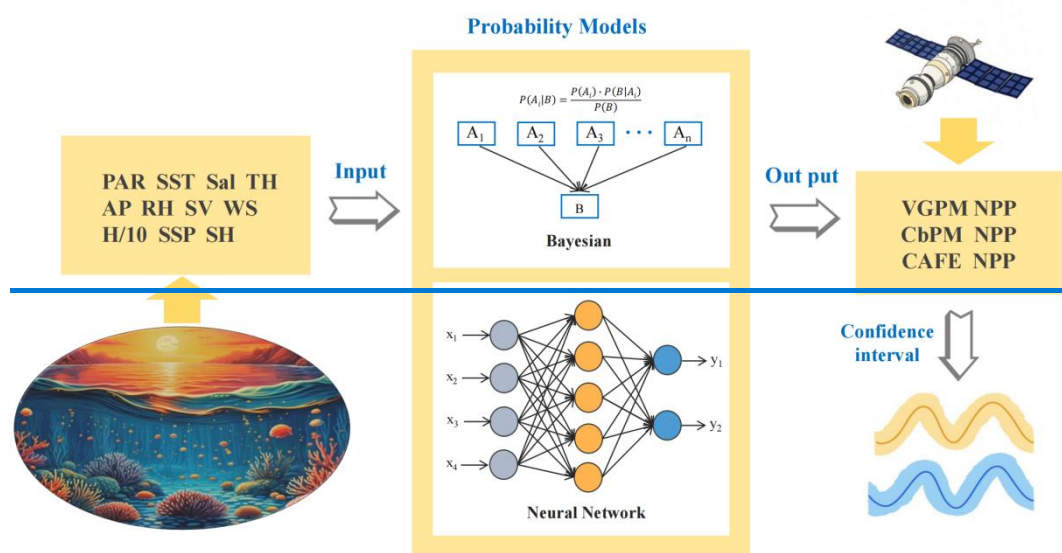
~~graphical abstract~~

1. Introduction

Net Primary Production (NPP) of phytoplankton, an essential indicator for biological productivity, exerts a substantial influence on global carbon flux and the dynamics of marine ecosystems (Yang et al., 2021; Silsbe et al., 2016). The precision in estimating NPP is primary for environmental quality assessments (Falkowski et al., 1998; Tan et al., 2005), effective fisheries resource management, and comprehending the impacts of global climate change (Lee et al., 2015; Ding et al., 2016). ~~Conventional methods of NPP measurement, such as ship-based sampling and bottle incubations, are beset with challenges like human errors and inadequacies in capturing spatial and temporal dynamics.~~ While acknowledging the contributions of conventional ship-based approaches to marine productivity research, it is important to recognize their limitations in capturing the full spectrum of temporal variability and fine-scale spatial heterogeneity. These methods often involve episodic sampling and may not provide the continuous data streams necessary for understanding rapid ecological changes. This underscores the necessity for more sophisticated and comprehensive methods (Yang et al., 2021; Li et al., 2020).

The advent of ocean observation satellites and ocean color remote sensing technology has catalyzed a paradigm shift in the estimation of large-scale marine primary productivity (Yang et al., 2021; Westberry et al., 2008). These pioneering technological advancements furnish novel insights into phytoplankton photosynthetic production and its essential role in the carbon cycle, thereby broadening the observational spectrum and establishing a robust foundation for predicting marine NPP. Initial remote sensing endeavors to estimate NPP, employing satellite-based chlorophyll-a (Chl-a) (Platt et al., 1991; Platt & Sathyendranath, 1988; Sathyendranath et al., 1995), stemmed from the established correlation between chlorophyll and photosynthesis (Ryther, 1956; Ryther & Yentsch, 1957). However, these efforts were predominantly confined to local or regional applications. A subsequent investigation by Campbell et al. (2002) delved into the accuracy of various satellite primary productivity algorithms, unveiling that estimates from the most effective algorithm often diverged

81 from those derived from those obtained using the ^{14}C isotope labeling method. Their

82 study also unearthed systematic biases in several algorithms, which could be alleviated

83 through re-parameterization. Satyendranath et al. (2020) emphasize the critical role of

84 accurately assigning parameters in primary production models as a key strategy for

85 reducing model uncertainties and enhancing the reliability of satellite-based primary

86 production estimates, particularly in the context of climate research.

87 Currently, the ~~most widely utilized models for estimating NPP include~~estimation

88 of NPP primarily relies on three mainstream models: the Vertically Generalized

89 Production Model (VGPM), the Carbon-based Productivity Model (CbPM), and the

90 Carbon, Absorption, and Fluorescence Euphotic-resolving ~~model~~Model (CAFE~~), have~~

91 ~~been~~). These models were successively proposed (~~by~~ Behrenfeld et al~~.,~~. (1997~~;~~),

92 Westberry et al~~.,~~. (2008~~;~~), and Silsbe et al~~.,~~. (2016~~).~~), respectively, and have become

93 benchmark methods in this research field. Spanning various decades, these models

94 address diverse facets of ocean primary production and are readily accessible via

95 satellite remote sensing data platforms. As a result, they have been extensively applied

96 and discussed in numerous studies (Westberry et al., 2008; Pan et al., 2012; Dave et al.,

97 2013; Li et al., 2020; Yang, 2021; Cael, 2021). Particularly, VGPM formulates a light-

98 dependent, depth-integrated model that classifies environmental factors influencing the

99 vertical distribution and optimal assimilation efficiency of primary production,

100 leveraging ^{14}C productivity measurement data (Behrenfeld et al., 1997). Conversely,

101 CbPM was a depth-resolved spectral NPP model designed for phytoplankton growth

102 rates (Westberry et al., 2008). Its foundational concept was originally articulated by

103 Behrenfeld et al. (2005). Distinguishing itself from Chl-based models, CbPM enables

104 the differentiation of physiological changes in biomass and Chl, thus offering a more

105 nuanced depiction of phytoplankton production. Notably, its strength lies in addressing

106 issues related to light and nutrient adaptation, thereby enhancing its capability in

107 estimating fixed carbon output at the ocean surface. Similarly, the CAFE model,

108 introduced in 2016, presents an adaptive framework that melds satellite ocean color

109 analysis with essential physiological and ecological attributes of phytoplankton (Silsbe

et al., 2016). It incorporates intrinsic optical properties into the model and calculates NPP by assessing the product of energy absorption and the efficiency of converting absorbed energy into carbon biomass, alongside computing growth rates. Nonetheless, these models commonly generate a single value of NPP, overlooking the range estimation and the inherent uncertainties in NPP estimation, stemming either from the model itself (BIPM et al., 2009) or from the model input (Milutinovic & Bertino, 2011). This oversight is critical, as suggested by Saba et al. (2011), since uncertainties in input variables, like Chl-a, significantly impinge upon model performance and accuracy. In a recent assessment, Westberry et al. (2023) examined the daily depth-integrated NPP rates over 2003–2018 for VGPM, CbPM, and CAFE, revealing that the mean NPP fields of CbPM and CAFE, along with their associated frequency distributions, are distinctly divergent from those of VGPM.

Transitioning from the constraints of traditional models, probabilistic forecasting, in contrast to deterministic forecasting (Juban et al., 2007), generates a cumulative distribution function or probability density function for the predicted object. This methodology offers a more holistic understanding of likely outcomes (Gneiting & Katzfuss, 2014; Schepen et al., 2018; Zhao et al., 2015). Significantly, this approach has been successfully implemented in fields such as hydrology (Schepen et al., 2018; Zhao et al., 2015; Schwanenberg et al., 2015) and power system management (Al-Gabalawy et al., 2021). For instance, Schwanenberg et al. (2015) conducted analyses using both deterministic and probabilistic forecasts. They concluded that deterministic forecasts tend to overlook forecast uncertainty in short-term decisions, whereas probabilistic forecasting offers numerous advantages: (i) it enables a longer forecast horizon, facilitating earlier and more accurate predictions of major events; (ii) it supports decision-making by incorporating forecast uncertainty into the analysis, leading to more robust and adaptive outcomes; and (iii) it enhances the flexibility of system operation through the integration of uncertainty-based methodologies.

The estimated values of NPP derived from the above three classical models

exhibit significant discrepancies, reflecting substantial uncertainties in these methods. These inaccuracies can impede a comprehensive understanding of the role of oceans in the global climate system, particularly in their capacity to act as carbon sinks and regulators of atmospheric CO_2 levels. Consequently, quantifying and addressing these uncertainties is primary to improving the reliability of NPP estimates and ensuring their applicability in climate research and marine ecosystem management. Although Bayesian models and probabilistic neural networks are established methods, their application to the remote sensing of marine net primary productivity (NPP) represents a novel approach. This study leverages these advanced probabilistic techniques to address the unique challenges in estimating NPP from satellite data, providing a more accurate and reliable quantification of uncertainties. We introduce probabilistic prediction models to meticulously quantify the uncertainty of NPP estimation, thereby enhancing our comprehension of NPP's significance in marine ecosystems. The research objectives of this paper are articulated as follows: (1) to thoroughly quantify the uncertainty of NPP estimation through the integration of probabilistic forecasting; (2) To evaluate and contrast the efficacy of neural network-based probabilistic forecasting with empirical distribution-based Bayesian probabilistic forecasting in capturing NPP uncertainty; and (3) To implement probabilistic forecasting of the uncertainty of the NPP in the study area during 2007–2018 and to explore its temporal characteristics. Our study offers innovative perspectives and methodologies for addressing the uncertainty associated with NPP. The organization of this paper is as follows: Section 2 outlines the study area and data sources; Section 3 elaborates on the methodology and presents metrics for evaluating forecasting performance; Section 4 discusses the results; and Section 5 presents the conclusions.

2. Data and Methods

2.1. Study Area and Data Sources

The research locale for this study is situated in the aquatic environs of Weizhou Island, nestled within the Gulf of Tonkin, Guangxi Province, southern China (Fig. 1).

The proportion of excellent water quality in Guangxi's near-shore waters reaches more than 90% all year round, and the quality of the marine ecological environment has remained at the forefront of the country for 12 consecutive years, which is the only stable habitat and feeding ground for large cetaceans known in China's near-shore waters at present. Weizhou Island is the youngest volcanic island in China geologically, with more than 95% of its strata comprising volcanic rocks. Its landscape features include formations resulting from sea erosion, marine sediment accumulation, and dissolved rocks. Weizhou Island, located in the southern subtropical monsoon zone, experiences a pleasant climate with abundant heat and precipitation throughout the year. The average annual temperature is 23°C, and the average winter temperature is 16.3°C. The island extends in a NE-SW direction and has an elliptical shape. It is approximately 6 km long from north to south, 5 km wide from east to west, and has an area of approximately 25 km^2, making it the largest and youngest volcanic island in China (Li and Wang, 2004). Weizhou Island is an inhabited volcanic island, the annual average water surface temperature is about 24° C, and ranges from 19° C to 30° C. The annual average seawater salinity is 32‰, seawater pH ranges from 8.0 to 8.23, and seawater transparency ranges from 3 m to 10 m (Yu et al., 2019). In addition, Weizhou Island is the northernmost island in the Gulf of Tonkin, where coral reefs have developed. These coral reefs are mainly found in shallow waters along the southwest, northwest, and northeast coasts, with widths ranging from 0.86 to 2.56 km (He and Huang, 2019). The unique climatic conditions and island landscape make it a popular tourist destination. The waters of Weizhou Island are the habitat of many rare marine organisms, and the protection and research of its marine ecosystem are of great significance to maintaining marine biodiversity.

The dataset of this study encompasses eight distinct sets of monitoring data spanning from January 2007 to February 2018, amassing a total of 4077 days. These data were procured from the Weizhou Marine Environmental Monitoring Station (21.0017°N, 109.0117°E) and encompass a spectrum of variables: sea surface temperature (SST), salinity (Sal), tide height (TH), air pressure (AP), relative humidity

(RH), sea visibility (SV), wind speed (WS), and 1/10th significant wave height (H/10). Additionally, photosynthetically active radiation (PAR) was retrieved from NASA's Ocean Color portal (https://oceancolor.gsfc.nasa.gov/), sea surface precipitation (SSP) was sourced from Nasa Earth Observation Data (~~https://www.earthdata.nasa.gov/~~https://www.earthdata.nasa.gov/), and sunshine hours (SH) was sourced from the China Meteorological Administration (https://data.cma.cn/). These data were aggregated to constitute a comprehensive dataset encompassing eleven variables, serving as the input features for the models. Phytoplankton, the primary source of NPP, is directly influenced by variables such as SST, Par, and SH, which are critical to its photosynthetic processes. Additionally, other variables have significant indirect effects on phytoplankton growth. Sal, for example, influences the community structure of phytoplankton (Braarud et al., 1951). Variables such as TH, H/10, and WS indirectly affect phytoplankton dynamics by modulating water column mixing and the vertical distribution of nutrients. AP, RH and SV also indirectly impacts phytoplankton photosynthetic activity by altering environmental conditions. For the analysis of three NPP algorithms—namely, VGPM, CbPM, and CAFE—we utilized their output datasets, which were obtained at an eight-day temporal resolution from the Ocean Productivity website (http://orca.science.oregonstate.edu/1080.by.2160.monthly.hdf.vgpm.m.chl.m.sst.php, ~~http://orca.science.oregonstate.edu/1080.by.2160.monthly.hdf.cbpm2.m.php,~~http://orca.science.oregonstate.edu/1080.by.2160.monthly.hdf.cbpm2.m.php, http://orca.science.oregonstate.edu/1080.by.2160.monthly.hdf.cafe.m.php). These datasets represent the modeled NPP estimates produced by each algorithm over a cumulative duration of 514 days. The specific datasets utilized for this study are itemized in Table 1.

Due to factors such as equipment malfunctions and adverse weather conditions, some data for the eleven variables were incomplete~~.~~, which may affect the accuracy of the model, especially when capturing extreme events. To gain a deeper understanding of the data structure and address these gaps, we conducted an analysis of the missing

data and identified five variables with missing entries (Table 2): SV, H/10, SSP, PAR, and SH. These missing data points are primarily due to random occurrences such as satellite equipment malfunctions and severe weather conditions, which disrupt data acquisition. Since these events are sporadic and not tied to any specific frequency, only the total number of missing values has been recorded. Subsequently, we visualized these five variables in a chronological sequence, with the findings depicted in Fig. 2. Distinct from daylength, which is computable based on location and date, SH indeed refers to the daily measured duration of sunlight reaching the Earth's surface. The variability and instances of zero values observed in Fig. 2 (bottom panel) and mentioned in Table 2 reflect real-world fluctuations due to weather conditions—on overcast or rainy days, actual sunshine hours recorded can indeed drop to zero. These data are collected on a daily basis, hence the seemingly sporadic pattern rather than a smooth temporal variation expected of constant daylength calculations. The analysis revealed a marked periodicity in these variables, prompting us to employ time series interpolation as our method of choice for data imputation. The efficacy of this approach is evidenced in Table 3, which presents the statistical indicators of the data both pre- and post-interpolation. Notably, while the post-interpolation data retains a close resemblance to the original data in terms of statistical indicators, it is important to acknowledge that interpolated data are not independent observations. The validity of the interpolation method, therefore, depends on the specific application and context. In this study, interpolation was used to address missing variables, and we ensure that the statistical properties of the original data were preserved to the greatest extent possible. This approach allows us to maintain the integrity of our analyses while recognizing the inherent limitations of using interpolated data.

VGPM, CbPM, and CAFE rely on similar input variables, derived from satellite observations and environmental measurements. VGPM uses inputs such as SST, chlorophyll concentration (Chl), and PAR to estimate NPP, leveraging optimal assimilation efficiency in its parameterization (Behrenfeld et al., 1997). CbPM focuses on phytoplankton carbon biomass, incorporating backscattering coefficients along with

Chl. CAFE integrates additional inputs, including atmospheric pressure (AP), solar heat (SH), and wind speed (WS), to parameterize light and nutrient availability critical for phytoplankton growth.

To evaluate the long-term trends in Net Primary Production (NPP), we applied a low-pass filter to the three NPP products (VGPM, CbPM, and CAFE) (Fig. 3). This filtering process removes high-frequency variations, such as noise and short-term fluctuations, while retaining the underlying long-term patterns. It became evident that each exhibits a distinct seasonal periodicity, with the fluctuation ranges remaining stable over time yet the magnitude and timing of them varing significantly among the three NPPs. Specifically, VGPM are the smallest, followed by CAFE, while CbPM have the largest values. This periodicity indicates that changes in NPP are not random but follow predictable laws and reflects the well-established seasonal patterns in marine primary production, associated with seasonal variations in environmental factors such as light availability, temperature, and nutrient. Such periodic trends are expected in regions around 21 degrees north, including the waters near Weizhou Island, due to the interplay of monsoonal influences and seasonal shifts in oceanographic conditions. While all three NPPs capture these periodic patterns, their representation of the magnitude and timing of peaks differs. The distinct ways in which VGPM, CbPM, and CAFE capture these patterns provide valuable insights into their respective model designs and parameterizations.

To elucidate the correlation between these NPP products and our dataset, we generated Pearson correlation plots (Fig. 4). The results revealed that the variables with the highest correlations differed among the three NPP values. Notably, VGPM showed the strongest correlation with SST, reflecting its dependence on sea surface temperature in its parameterization. Both CAFE and CbPM showed strong correlation with AP, albeit in opposing directions—CAFE displayed a positive correlation, while CbPM NPP exhibited a negative one. Changes in AP affect atmospheric stability, cloudiness, and precipitation, indirectly altering light conditions in the ocean and subsequently

affecting phytoplankton photosynthesis. Lower AP often corresponds to unstable atmospheric conditions and increased cloud cover, which may inhibit photosynthesis activity by reducing light penetration. Additionally, phytoplankton dynamics modeled in CbPM may respond differently to such changes compared to CAFE, potentially due to the distinct assumptions and parameterization used in each model. In summary, among the three models, VGPM possesses the most significant correlation with the variables, followed by CAFE, and lastly CbPM.

2.2. Methods

2.2.1. Bayesian Probability Prediction

Bayesian models can adeptly quantify the uncertainty in the distribution of predicted outcomes. The Bayesian approach is particularly advantageous in scenarios with limited training data or when potential invisibility in training data cannot be discounted in practical applications (Perfors et al, 2011; Kaplan D, 2021; Zou et al, 2024). The Bayesian formula is represented as:

$$P(\theta|D) = \frac{P(D|\theta) \cdot P(\theta)}{P(D)} \tag{1}$$

where

$$P(\theta|D) = \frac{P(D|\theta) \cdot P(\theta)}{P(D)} \tag{1}$$

where θ denotes the model parameters, and D represents the training dataset, $P(\theta|D)$ denotes the posterior probability, $P(D|\theta)$ the likelihood probability, $P(\theta)$ the prior probability, and $P(D)$ the marginal probability for normalization.

When a training dataset D is available, the probability distribution $P(\theta|D)$ of θ is computable using the aforementioned Bayesian formula (Dürr et al, 2020). To deduce $P(\theta|D)$, it is imperative to ascertain the likelihood probability $P(D|\theta)$ of the observed data under the model parameter θ. $P(D|\theta)$ can also be interpreted as the probability of obtaining the training dataset D given parameter θ. Additionally, knowledge of the prior

probability $P(\theta)$ and the evidence $P(D)$ is essential. Given that the training dataset D is fixed, $P(D)$ remains constant. Consequently, the posterior distribution is proportional to the likelihood probability multiplied by the prior distribution, i.e., $P(\theta|D) \propto P(D|\theta) \cdot P(\theta)$, in accordance with Bayes' Law.

In this study, the Bayesian approach is employed to calculate the posterior distributions of the parameters considering the prior information and the input data. Subsequent predictions are made using the posterior distributions, yielding a probability distribution for each predicted value. Ultimately, the model's ability to estimate the uncertainty in the NPP is illustrated by plotting the prediction ranges for different targets and comparing them to actual observations.

2.2.2. Neural Network Probabilistic Prediction Model Based on TFP

TensorFlow Probability (TFP) represents a sophisticated library of statistical algorithms, devised atop the TensorFlow Python API. Its primary objective is to streamline the integration of probabilistic models with deep learning frameworks. TFP offers a comprehensive suite of tools, enabling the construction of probabilistic models adept at estimating uncertainty. Aiming to thoroughly assess the predictive efficacy of the three NPP products, we employed a neural network model grounded in the TFP framework, capitalizing on its versatility and potent expressive capabilities for probabilistic prediction in marine ecosystems.

The architecture of this neural network model incorporates multiple hidden layers, each implementing a nonlinear transformation via an activation function. Such a configuration enables the model to automatically extract higher-order features and intricate patterns from the data. Our selection of TFP as the implementation medium allows us to model the neural network's output by integrating probability distributions, thus addressing the model's uncertainty regarding predictions and yielding more exhaustive insights. Specifically, our neural network model utilizes a distribution layer in the output stage, producing a probabilistic distribution concerning the target variable,

as opposed to a mere deterministic point prediction. This probabilistic output facilitates the quantification of the model's confidence level for each prediction, extending beyond mere point estimates.

The integration of Bayesian models and probabilistic neural networks in our approach addresses key challenges in the remote sensing of NPP. These challenges include handling the variability and uncertainty inherent in satellite-derived data and environmental factors, thus improving the robustness of NPP estimates. In this study, the input variables for the models are the 11 environmental variables mentioned in Section 2.1, and the outputs are VGPM, CbPM, and CAFE. These inputs variables partially overlap ~~substantially~~ with those used in VGPM, CbPM, and CAFE~~, demonstrating that the NN and Bayesian models do not require additional or more complex inputs~~. The selection of input data was not limited to variables directly related to phytoplankton photosynthesis, such as SST, PAR, and SH. Instead, it also included a wide range of environmental variables that could influence phytoplankton growth, such as TH, WS, and AP, which are physical dynamics and meteorological characteristics. Since phytoplankton are the primary source of NPP, environmental factors affecting phytoplankton growth also indirectly impact NPP. These emphasize the variability in how different NPP models capture environmental interactions. Importantly, the Pearson correlation analysis (Fig. 4) highlights the most relevant variables for prediction, enabling the NN and Bayesian models to focus on key inputs and filter out less influential variables.

The dataset spans 4,077 days, but due to the 8-day time interval of the downloaded NPP products, only 514 complete datasets are available for model training and performance evaluation. Given the limited amount of data, 80% of the 514 sets are used for model training and parameter tuning, while the remaining 20% are used for performance evaluation. In the neural network probabilistic prediction model, there are six layers, with two output nodes used to estimate the mean and standard deviation. The Gaussian distribution is employed in the distribution layer, and the loss function is the

negative log-likelihood loss function. The detailed parameters of the neural network are presented in Table 4.

2.3. Model Evaluation

Prior to model evaluation, we normalized the NPP satellite data. This step is critical to improving model performance because it removes the potential effects of different data scales, allowing the model to consider each data point more fairly. Normalization ensures that the distribution range of NPP data has the same weight during model training, thus improving the model's ability to capture the inherent patterns and features of the data. In addition, normalization helps reduce the noise and bias introduced by data scale differences, further enhancing the stability and predictive accuracy of the model.

Before training the model, we divided the dataset reasonably. Specifically, we divided the dataset into 80% training set and 20% testing set. This division aims to ensure that the model can fully learn the features and patterns of the data during the training process, while retaining enough independent data for testing the predictive ability of the model. This way of dividing the dataset helps us to evaluate the performance of the model more accurately and avoid problems such as overfitting.

In this study, our models provide probabilistic predictions, generating a probability distribution for each time point rather than a single point estimate. To facilitate visualization and interpretation, the curves presented in some figures represent the mean values derived from these predictive distributions. These mean curves summarize the central tendency of the model outputs while inherently accounting for the uncertainty associated with the predictions.

2.3.1. CDF

The Cumulative Distribution Function (CDF), also known as the distribution function, is the integral of the probability density function (PDF). It provides a complete

description of the probability distribution of a real-valued random variable X. The CDF is defined as the probability P that a random variable X is less than or equal to a given value x, expressed as:

$$F(x) = P(X \leq x) \tag{2}$$

To evaluate the predictive performance of the model, we computed the empirical CDF of the input data and compared it with the average predictive CDF generated by the model. This comparison provides a graphical representation of the model's predictive accuracy. A higher degree of overlap between the empirical and predictive CDF curves indicates a greater similarity between the two distributions, thereby reflecting superior model predictions.

2.3.1. 2.3.2. CRPS

In probabilistic forecasting, the focus extends beyond mere point estimates to encompass the shape and dispersion of the probability distribution. Hence, traditional scoring functions prove inadequate, as aggregating the predicted distributions into their mean or median neglects critical information about the dispersion and shape. Continuous Ranked Probability Score (CRPS)Continuous Ranked Probability Score (CRPS), by embracing the entire probability distribution, emerges as an invaluable tool in assessing model uncertainty. CRPS is a sophisticated statistical metric employed to evaluate the efficacy of forecasting models. Initially introduced in the 1970s (Matheson & Winkler, 1976), CRPS is widely utilized in areas such as weather forecasting (Zamo et al., 2018). It quantifies the divergence between the predicted probability distribution and the actual observations (Hersbach, 2000). Ideally suited for scenarios where the target variable is continuous and the model predicts its distribution (Pic et al., 2023), CRPS equates to the mean absolute error (MAE) in deterministic forecasting (Zhao et al., 2015).

In probabilistic forecasting, the focus extends beyond mere point estimates to

encompass the shape and dispersion of the probability distribution. Hence, traditional scoring functions prove inadequate, as aggregating the predicted distributions into their mean or median neglects critical information about the dispersion and shape. CRPS, by embracing the entire probability distribution, emerges as an invaluable tool in assessing model uncertainty. CRPS is calculated as follows:

1. For each sample (individual data points in the dataset, each representing a specific combination of environmental conditions and corresponding NPP estimates), calculate the discrepancy between the cumulative distribution function (CDF) of the predicted and observed values.

2. Aggregate the variances for all samples and divide by the number of samples to obtain the average variance.

$$CRPS_{individual}(F,x) = \int_{-\infty}^{+\infty}[(F(y) - H(y - x)]^2 dy \qquad (2(F,y) =$$

$$\int_{-\infty}^{+\infty}[(F(x) - H(x - y)]^2 dx \qquad (3)$$

$$CRPS = \frac{1}{n}\sum_{i=1}^{n} CRPS_{individual}(F_i, x_i y_i) \qquad (3\underline{4})$$

where $F(y x)$ denotes the CDF of the predicted value, $y x$ the predicted value, $x y$ the observed value, and $H(x-y x)$ the Heaviside function which is 0 when $x \leq y < x$ and 1 otherwise. n indicates the total number of samples, and $CRPS_{individual}(F_i, x_i y_i)$ the CRPS value for the i-th sample.

A smaller CRPS value signifies a closer alignment of the model's probability distribution with actual observation, integrating insights on both the shape and location of the distribution and demonstrating sensitivity to outliers. Unlike other metrics such as Root Mean Square Error (RMSE) or Mean Absolute Error (MAE), CRPS offers a more holistic evaluation of a probability distribution's predictive capacity by considering the full distribution shape. For Bayesian and neural network models, comparing CRPS values facilitates an understanding of their proficiency in fitting the

438 entire probability distribution.

439 ~~2.3.2.~~ 2.3.3. ~~CDF~~

440 ~~The Cumulative Distribution Function (CDF), also known as the distribution~~
441 ~~function, is the integral of probability density function (PDF). It provides a complete~~
442 ~~description of the probability distribution of a real-valued random variable *X*. The CDF~~
443 ~~is defined as the probability *P* that a random variable *X* is less than or equal to a given~~
444 ~~value *x*, expressed as:~~

445 $$F(x) = P(X \leq x) \tag{4}$$

446 ~~To evaluate the predictive performance of the model, we computed the empirical~~
447 ~~CDF of the input data and compared it with the average predictive CDF generated by the~~
448 ~~model. This comparison provides a graphical representation of the model's predictive~~
449 ~~accuracy. A higher degree of overlap between the empirical and predictive CDF curves~~
450 ~~indicate a greater similarity between the two distributions, thereby reflecting superior~~
451 ~~model predictions.~~

452 ~~2.3.3.~~ RMSD

453 Root Mean Squared Deviation (RMSD) is a widely recognized evaluation metric
454 in regression analyses, primarily employed to quantify the discrepancy between a
455 model's predicted values and the actual observed values. Characterized by its intuitive
456 nature and simplicity in computation, RMSD is particularly beneficial in scenarios
457 where emphasis is placed on the magnitude of difference between predicted and actual
458 values, irrespective of the difference's direction.

459 $$RMSD = \sqrt{\frac{1}{n}\sum_{i=1}^{n}(y_i - x_i)^2} \tag{5}$$

460 where n denotes the number of samples, y_i represents the predicted value of the *i-th*
461 sample, and x_i symbolizes the actual value of the *i-th* sample.

462   A lower RMSD value is indicative of superior model performance, signaling a

463 smaller variance between the model's predictions and the observed values. Nevertheless,

464 it is important to note that RMSD exhibits sensitivity to outliers, as it constitutes the

465 mean of the squared differences. Incorporating RMSD alongside CRPS in our analysis

466 enables a more comprehensive evaluation of both the overall accuracy and uncertainty

467 inherent in the predictions.

468   ~~2.3.4.~~   2.3.4. MAPD

469   Mean Absolute Percentage Deviation (MAPD) is a frequently utilized percentage

470 error metric in regression problems. It expresses the prediction error as a percentage,

471 offering an insightful perspective into the relative error between predicted results and

472 true values in predictive model evaluations.

473
$$MAPD = \frac{1}{n}\sum_{i=1}^{n}\left|\frac{x_i - y_i}{x_i}\right| \times 100\% \tag{6}$$

474 where n signifies the number of samples, y_i the predicted value of the *i-th* sample, and

475 x_i the actual value of the *i-th* sample.

476   A lower MAPD value is desirable, indicating a reduced relative error of the model.

477 However, a cautionary note: MAPD may prove unreliable in instances where the

478 predicted value approaches zero, as a zero denominator results in infinity. Therefore,

479 careful consideration is warranted when employing MAPD, particularly in scenarios

480 where relative accuracy is primary.

481   In the context of comparing Bayesian probabilistic prediction models with neural

482 network probabilistic prediction models, the synergistic application of these three

483 metrics—CRPS, RMSD, and MAPD—affords a multifaceted assessment of the models.

484 This triad of metrics enhances our understanding of the importance of relative error

485 alongside the accuracy of point estimates and the fit of probability distributions.

486 **3. Results and Discussion**

3.1. Comparative Analysis of Prediction Efficacy Between Two Models

We utilized VGPM, CbPM, and CAFE as prediction targets to scrutinize the predictive effectiveness of both the neural network-based probabilistic prediction model and the empirical distribution-based Bayesian probabilistic prediction model. Fig. 5 presents a comparison of CRPS, RMSD, and MAPD values for both NN and Bayes models using three NPPs as prediction targets across training and test datasets. Notably, CRPS provides a holistic evaluation of prediction accuracy and reliability. All the metrics are calculated using normalized data for better comparison. Lower values are indicative of enhanced model performance. Fig. 5(a)-(c) and (d)-(f) respectively depict the CRPS, RMSD, and MAPD of the NN model and Bayes model when using the three NPP values as prediction targets. The color blue represents the training set, while red represents the test set.

It can be observed from Fig.5 (a) and (d) that the CRPS values of both the NN model and Bayes model are similar. When VGPM is used as a prediction target, the performance of the models is closest between the training set and test set, followed by CbPM. However, CAFE has the lowest CRPS value among all three models, with its test set slightly larger than that of its training set. The lower CRPS value for the CAFE NPP, compared to VGPM and CbPM, may stem from the fact that its probability distribution aligns more closely with the prediction of models in terms of both shape and central tendency, since CRPS evaluates the full probability distribution, incorporating factors such as skewness and kurtosis in addition to variance. In the case of CAFE, the probabilistic structure of its predictions may exhibit better congruence with the observed cumulative distribution function (CDF) (Section 3.2.21), particularly in regions with higher data density. This enhanced alignment could compensate for its slightly larger variance compared to CbPM, thereby resulting in a lower CRPS value. Additionally, the design and parameterization of the CAFE model may inherently emphasize features that lead to improved probabilistic predictions, which warrants further investigation.

In terms of RMSD metrics (Fig. 5 (b) and (e)), when VGPM is used as a prediction target, its index value is significantly higher compared to others; however, its performance between training set and test set remains close. When CbPM is used as a prediction target, Bayes model outperforms NN model but exhibits a larger difference between training set and test set compared to NN model.

Regarding the MAPD indices (Fig. 5 (c) and (f)), it can be seen that there is a significant difference between the NN and Bayesian models when the three NPP values are used as the prediction targets, respectively, where the MAPD values are significantly lower when CAFE is used as the prediction target than when CbPM and VGPM are used as the prediction targets. In addition, for the NN model, the MAPD index value for CAFE is lower than that of the Bayes model. However, there exists significant difference between its training set and test set.

It is critical to note that our uncertainty quantification framework focuses on propagating uncertainties from the base models (VGPM, CbPM, CAFE) through the emulation process, rather than assessing the structural adequacy of these models themselves. The neural network and Bayesian models developed in this study were trained using outputs from the VGPM, CbPM, and CAFE models. While this approach allowed us to evaluate the uncertainty in emulating these base models, it also means that our models inherit their underlying biases and errors. As such, the uncertainty estimates reported here reflect the uncertainty in emulating these specific outputs and do not represent the true uncertainty of NPP estimation. Furthermore, as Fig. 3 demonstrates, the outputs of VGPM, CbPM, and CAFE differ significantly, underscoring the need for ground truth data to validate these models. Among these, CAFE NPP is often considered more accurate based on prior studies, but further validation with observational data is necessary to confirm this assumption.

On using CAFE as a prediction target, both models show more consistent performance. The values of these indicators are relatively close in all aspects at around 0.2. Regarding MAPD metrics (Fig.5 (c) and (f)), clear differences among the three

NPP models can be seen where CAFE has obviously lower index value compared to CbPM and VGPM. In addition, for NN model's MAPD index value for CAFE is lower than that for Bayes model. However there exists significant difference between its training set and test set.

Overall evaluation indicates that under both models' assessment criteria, CAFE demonstrates superior accuracy in predicting effects compared to VGPM and CbPM. VGPM shows greater instability with inferiority in its training process over testing process (Fig.5 (d), (e), (f)), which may be attributed to overfitting. However, there is a more noticeable difference in the performance of CbPM in the two models. The CRPS value and RMSD value in the Bayes model are significantly lower than those in the NN model (Bayes is less than 0.2, while NN is more than 0.2).

Therefore, among the three NPP datasets (VGPM, CbPM, and CAFE), the CAFE was selected as the primary prediction target for subsequent analysis. This decision was motivated by two factors: (1) prior research indicatingPrevious studies have shown that CAFE provides relatively accurate estimates of for other NPP in marine ecosystems with characteristics similar tomodels analyzed for the Weizhou Island area, due to its advanced parameterization of phytoplankton dynamics,same dataset, the CAFE model explains the most variance and has the lowest model bias, and also reproduces the magnitude and seasonality of field-measured NPP better than other satellite remote sensing models(Silsbe et al., 2016), and (2) the demonstrated ability of both probabilistic prediction models (NN and Bayesian) to emulate CAFE output with high accuracy and reliability. While this does not imply that CAFE perfectly represents true NPP, its suitability for capturing patterns in the study area supports its use as the prediction target in this work.

3.2. Quantify the Uncertainty of CAFE

When quantifying uncertainty in the CAFE, we need to focus on the uncertainty factors that exist in the input variables in addition to the uncertainty that may arise

during model training. These uncertainty factors include measurement errors and temporal variability, among others. Measurement errors usually originate from the accuracy limitations of the instruments, the complexity of the observation environment, or the instability of human operations. These errors not only affect the accuracy of the input variables to varying degrees, but also propagate through the model and thus affect the accuracy of the prediction results. The temporal variability, on the other hand, reflects the dynamic changes of marine environmental parameters, such as seasonal temperature changes, cyclic fluctuations of tides, etc., which also affect the NPP prediction results. Consequently, quantifying these uncertainties is particularly important in conducting CAFE predictions.

3.2.1. Comparative Analysis of Confidence Interval Widths

Fig. 6 illustrates the comparison between the forecast mean of the NN model and Bayes model, and the CAFE value when CAFE is utilized as the prediction target. In the figure, the triangular icons represent 514 sets of the forecast average, while the gray and blue represent the 95% and 75% confidence intervals, respectively. Overall, both models exhibit relatively wide confidence intervals for their predicted results, possibly due to the large range of changes in CAFE. The models may face greater challenges in capturing this wide range of changes, resulting in increased uncertainty.

When CAFE is less than 450 mg C m^{-2} d^{-1}, both models tend to overestimate the actual NPP value. This phenomenon becomes more pronounced when CAFE is less than 350 mg C m^{-2} d^{-1}. In contrast, a certain linear relationship between true value and predicted mean value emerges within a range of 450-600 mg C m^{-2} d^{-1}. Most of the predicted mean values are distributed around the 1:1 line in this range, indicating higher accuracy by these models. However, when CAFE exceeds 600 mg C m^{-2} d^{-1}, it is observed that both models tend to underestimate actual NPP values. This phenomenon may be attributed to an imbalance in sample data distribution within different intervals of CAFE. The majority of data points are concentrated in a narrow range (350-600 mg C m^{-2} d^{-1}), while data points in other intervals are scarce. This inadequacy makes it difficult for model training to capture its distribution law accurately and leads to

599   increased prediction uncertainty within these ranges.

600   Compared with the two models, the predicted value of NN model is more
601   concentrated around the 1:1 line, while the predicted value of Bayes model is relatively
602   dispersed and the confidence interval is wider. The smaller the confidence interval
603   width, the higher the accuracy of model prediction. It manifests that the NN
604   probabilistic prediction model is more accurate in predicting CAFE than the Bayes
605   probabilistic prediction model, and the uncertainty of its prediction results is lower. The
606   prediction mean obtained by the NN probabilistic prediction model is closer to the 1:1
607   line, which usually means that the deviation between the predicted value of the model
608   and the actual observed value is small, that is, the prediction accuracy of the model is
609   higher. The differences in the performance of the two models may stem from their
610   different strategies for dealing with uncertainty and data fitting. Neural network models
611   typically capture the nonlinear relationships of data through a large number of
612   parameters and complex network structures, so they may be able to fit the data
613   distribution more accurately in some cases. Bayes model deals with uncertainty by
614   introducing prior knowledge and a posteriori inference, but its performance may be
615   limited under some complex data distributions.

616   To further elucidate the models' effectiveness in probabilistic prediction of CAFE,
617   Fig. 7 visualizes the time series model predictions with a 95% confidence interval
618   uncertainty range. The figure shows that almost all CAFE values fall within the 95%
619   confidence interval of the mean of the predicted values. It can be clearly seen that the
620   predicted distribution of the NN model is much smaller than that of the Bayes model,
621   which is consistent with the results shown in Fig. 6. The NPP is clearly periodic in time,
622   and both models are able to align their predictions on the test set with the periodicity of
623   the training set. In particular, the scatter in the NN model is more centrally distributed
624   around the red line, while the scatter in the Bayes model is more discrete from the red
625   line, which further suggests that the NN model has a more accurate estimate in
626   predicting the CAFE.

627   Overall, the trends in the predicted means of the two models are consistent with

628   the trends in the majority of CAFE values, which further validates the accuracy of the

629   two methods in capturing the process of CAFE changes. This consistency not only

630   indicates that the models can accurately reflect the long-term trends of CAFE changes,

631   but also capture short-term fluctuations and outliers. This is of great significance for

632   ecosystem monitoring and prediction, and helps to better understand the dynamics of

633   the ecosystem and take appropriate management and conservation measures. However,

634   in terms of confidence interval width, the width of the 95% confidence interval in the

635   results of the Bayesian probabilistic prediction model is larger than that of the neural

636   network probabilistic prediction model, indicating that the Bayesian probabilistic

637   prediction model is not as sharp as the neural network probabilistic prediction model,

638   which is more locally sensitive and able to respond to the changes in data more quickly.

639   Although the neural network probabilistic prediction model shows an advantage

640   in terms of sharpness and local sensitivity, this does not mean that it is superior to the

641   Bayesian model in all cases. In fact, Bayesian models are more robust and explanatory

642   by introducing prior knowledge and posterior inferences to deal with uncertainty.

643   Therefore, when choosing a predictive model, trade-offs need to be made based on

644   specific application scenarios and data characteristics.

645   3.2.2. Comparative Analysis of CDF

646   Fig. ~~8 depicts the overall predictive distribution versus the empirical distribution~~

647   ~~of the CAFE input data. Concurrently, Fig. 9 methodically quantifies the disparity~~

648   ~~between the average predictive CDF and the empirical CDF of the input data. Optimally,~~

649   ~~the divergence between these two CDFs should be minimal, manifested as extensive~~

650   ~~overlap between the yellow and blue curves in Fig. 8, and the blue curve in Fig. 9~~

651   ~~approaching zero. Fig.~~ 8 demonstrates the CDF curves of the predicted mean values

652   after the normalization process and the CDF curves of the CAFE. The CDF plots of the

653   normalized data can reflect the statistical distribution of the datasets, especially when

654   the different datasets have different magnitudes or scales, and the normalization can

655   eliminate these differences, which makes the comparisons and analyses between the

656   different datasets more accurate and intuitive. Fig. 9 specifically quantifies the

difference between the two CDF curves in Fig. 8 at each point, which is accomplished

by calculating the difference between the y-values of the two CDF curves at the same

x-value. Optimally, the divergence between these two CDFs should be minimal,

manifested as extensive overlap between the yellow and blue curves in Fig. 8, and the

blue curve in Fig. 9 approaching zero.

While the cumulative distribution function (CDF) curves in Fig. 8 show apparent

differences between the test and train datasets for CAFE, these differences can

primarily be attributed to the smaller size of the test dataset relative to the training

dataset. Such size discrepancies can cause the CDF curves to appear visually different,

even when the underlying data distributions are similar. Moreover, as shown in Fig. 7,

the patterns for simulating the training set and predicting the test set are consistent for

both the NN and Bayesian models. This consistency indicates that the models

generalize well to the test data, capturing its key characteristics despite the visual

differences in the CDF curves. Therefore, the observed discrepancy in the CDF curves

does not imply poor representation of the test data by the training data. For the NN

probabilistic prediction model, when the CAFE values are lower, the two CDF curves

on the training set and the test set move gently and almost overlap, with the difference

close to 0, which indicates that the model can predict the actual data distribution well

within the range of small values of CAFE. As CAFE increases, the difference between

the predicted and true CDF curves grows larger, with the predicted mean CDF on the

training set generally lying below the CAFE CDF. The difference between the two

ranges from 0 - 0.2. For the test set, the predicted mean CDF initially slightly lies below

the true CDF curve at lower values, becomes steeper and overestimates at mid-range,

and alternates again at higher values. While these trends suggest some instability in the

model's predictions for higher values, the absolute difference between the two CDFs

remains within 0.1, indicating limited deviation. It is worth noting that the scatter plot

in Fig. 6 shows the test mean NPP predictions distributed more evenly around the 1:1

line. This apparent discrepancy arises from the differing perspectives of the two plots:

the CDF curve highlights cumulative differences across the distribution, whereas the

scatter plot reflects point-wise deviations. Together, these visualizations suggest that

687 while the model captures the overall distribution trends well, some localized errors in

688 predicting mid-range and higher values may contribute to these patterns.

689   For the Bayesian probabilistic prediction model, the predicted mean CDF curve is

690 above the true value in the training set. When the CAFE increases to a certain extent,

691 the two curves alternate, and the absolute value of the difference between the CDF does

692 not exceed 0.2. In the test set, the two CDF curves overlap first and then separate. The

693 predicted mean CDF rises more quickly, and is on top of the true value CDF curve, with

694 the difference between the two curves not exceeding 0.1 when the CAFE increases to a

695 certain extent. When the NPP increases to a certain degree, the two curves overlap again,

696 and the absolute value of the difference between the CDF does not exceed 0.3. Overall,

697 the difference between that of the predicted mean values and the CDF of the true values

698 obtained by the two models is small, which indicates that the overall deviation of the

699 model predictions is not large, and both models show good prediction performance and

700 can capture the statistical characteristics of the data well. However, the CDF curves of

701 the neural network probabilistic prediction model are closer to the true values on both

702 the training and test sets, possibly implying that the neural network model is more

703 effective in dealing with complex data and capturing nonlinear relationships. The

704 flexibility of neural networks allows them to adapt to different data distributions and

705 patterns.

706   Table 5 presents RMSD, MAPD, and CRPS for both models using CAFE as

707 prediction target. Additionally, we analyzed the proportion of raw input data

708 encompassed within the 95% confidence interval, thereby providing a more nuanced

709 evaluation of the model's proficiency in capturing CAFE uncertainty. According to

710 Table 5, the neural network-based probabilistic prediction model exhibits superior

711 performance in terms of CRPS, RMSD, and MAPD. This denotes a higher level of

712 accuracy and reliability for the neural network model in probabilistic predictions of

713 CAFE, especially when considering uncertainty. Conversely, the Bayesian probabilistic

714 prediction model demonstrates a stronger ability to encompass a greater proportion of

715 the raw input data within the 95% confidence interval. This suggests that while it may

exhibit higher overall uncertainty, it has a more pronounced capability to capture the nuances of uncertainty.

This comparative analysis elucidates that both the neural network-based probabilistic prediction model and the Bayesian probabilistic prediction model, grounded in empirical distributions, are adept at capturing and quantifying the uncertainty of CAFE. While the Bayesian model demonstrates a heightened capability in encompassing a broader scope of uncertainty, the neural network model distinguishes itself by its superior accuracy and reliability, particularly in precisely predicting the uncertainty of CAFE. A notable observation is that when CAFE values exceed 350 mg $C\,m^{-2}\,d^{-1}$, the predictive performance of both models deteriorates. This manifests as an underestimation of mean predictions, indicating an inability to fully and accurately predict NPP across the entire range of size classes. The underlying reason for this may stem from the considerable variation in the input data and its skewed sample distribution. Most notably, a significant proportion of the samples were primarily concentrated within the 200-350 mg $C\,m^{-2}\,d^{-1}$ range. In contrast, CAFE values exceeding 350 mg $C\,m^{-2}\,d^{-1}$ constitute only 28% of the input dataset. Consequently, the models exhibit insufficient learning of higher value ranges during the training phase, resulting in a notable prediction bias for larger CAFE values.

3.3. Probabilistic Prediction of NPP in Weizhou Island (2007–2018)

Given the 8-day temporal resolution of data acquired by remote sensing satellites and the consequent data incompleteness, this study employed the previously trained neural network and the Bayesian probabilistic prediction models using CAFE as training target to forecast the daily NPP in the Weizhou Island sea area from 2007 to March 2018, thereby supplementing the NPP dataset. This approach aligns with the focus established in Section 3.1, which emphasizes the efficacy of probabilistic prediction models when CAFE is used as the prediction target. The selection of CAFE outputs reflects the model's relative strengths in representing phytoplankton-based NPP dynamics in the study area, as well as the high accuracy achieved by the NN and

Bayesian models in emulating its output. The results are illustrated in Fig. 10, where the predicted mean values and 95% confidence intervals for both models are displayed. Fig. 10(c) reveals that the Bayesian model's confidence interval is broader, primarily due to its lower limit, yet no substantial difference is noted between the predicted mean values of the two models. Both models effectively mirror the trend of NPP. The analysis of the annual change of NPP shows a clear periodicity, which means that the change of NPP is not random, but follows certain laws and patterns. Combined with Fig. 11, the seasonal variation of NPP throughout the year emerges. Specifically, NPP shows a decreasing trend from January to July each year, with July generally being the lowest level of the whole year. Then it increases from July to November and slightly decreases from November to December. Overall, NPP has larger values in winter and spring. These results provide important insights into seasonal variations and interannual trends of NPP in the Weizhou Island waters and provide valuable data to support the study of the marine ecosystem dynamics.

However, the significance of our work extends far beyond mere data replication. The primary aim of our study is to enhance the reliability of marine NPP estimates by using advanced probabilistic models. Our objective extends beyond merely reproducing satellite NPP products. We aim to ~~improve~~enhance the ~~overall~~ accuracy and uncertainty ~~quantification~~ characterization of NPP estimates ~~by incorporating a robust probabilistic~~ within the current modeling framework, which focuses on quantifying uncertainties propagated from satellite products, input variability, and predictive model parameters. This framework helps to better understand and quantify the uncertainties inherent in marine NPP, whether they originate from satellite data or environmental factors. By using Bayesian models and probabilistic neural networks, we not only replicate satellite NPP estimates but also capture and quantify uncertainties at multiple levels. These models account for uncertainties in the satellite products, input data variability, and the predictive model itself, thus providing a more comprehensive uncertainty quantification relevant to marine NPP. However, it is important to acknowledge that structural uncertainties inherent in the base models (VGPM, CbPM,

CAFE) remain unquantified in this study. These could potentially introduce systematic biases undetectable by our current probabilistic framework, necessitating future multi-model ensemble approaches to address this limitation.

4. Conclusion

This study primarily addresses the challenge of uncertainty in satellite ocean color data estimates of ocean NPP. Departing from traditional point estimation regression models, we embraced a probabilistic prediction approach where the output is a probability distribution. The models utilized in this study include a Bayesian probabilistic prediction model based on empirical distributions and a deep learning-based probabilistic prediction model under the TFP framework. Focusing on the NPP uncertainty analysis in the Weizhou Island sea area, we explored the effect of the probabilistic prediction model when the NPPs obtained by the VGPM, CbPM, and CAFE methods, respectively, are used as the prediction targets. Unlike traditional models such as VGPM, CbPM, and CAFE, the NN and Bayesian probabilistic models are designed to capture complex nonlinear interactions between environmental variables and NPP while providing robust uncertainty quantification. ~~These probabilistic models do not require additional input variables beyond those used by VGPM, CbPM, and CAFE. Moreover, Pearson correlation analysis allows for the identification of the most critical inputs for prediction. By prioritizing variables such as SST and AP, the models can be optimized to reduce reliance on less influential inputs, improving efficiency without compromising accuracy.~~ Furthermore, this study compares and analyzes the capabilities of Bayesian and neural network probabilistic models in predicting the CAFE uncertainty. The results reveal that both models ~~are~~aDue to factors such as eqre competent in quantifying CAFE uncertainty.

When exploring the uncertainty of the NPP using the Bayesian probabilistic prediction model and the neural network probabilistic prediction model, the results show that the two probabilistic prediction models are the most effective when the prediction target is the CAFE. The probability distributions obtained by the two

probabilistic prediction models are similar to those of CAFE, with the difference in CDF between the predicted mean and true values at each data point not exceeding 0.2 for the neural network probabilistic prediction model and 0.3 for the Bayesian probabilistic prediction model. In contrast, the confidence intervals for the outputs of the Bayesian probabilistic prediction model are wider, and the proportion of the CAFE that falls in the confidence intervals is higher, which shows that Bayes is more capable of capturing uncertainty, but its accuracy is not high. However, the neural network probabilistic prediction model is more accurate and reliable. Its performance is better in many assessment indicators, but not all CAFE values in the size range can be predicted accurately by the model. When the CAFE is less than 450 mg C m^{-2} d^{-1}, the model tends to overestimate the actual NPP value. When CAFE is larger than 600 mg C m^{-2} d^{-1}, it tends to underestimate the actual NPP value. When the two probabilistic prediction models are applied to the prediction of CAFE in the Weizhou Island waters between January 2007 and February 2018, the prediction results illustrate the interannual trend of CAFE, and the magnitude of NPP is found to show obvious cyclic changes. Our study demonstrates the novel application of advanced probabilistic models to the remote sensing of marine NPP. Unlike climatological models that prescribe fixed uncertainties, our probabilistic framework dynamically adjusts prediction confidence in response to environmental disturbances. Its strengths lie in dynamic uncertainty quantification and multi-source data fusion capabilities. By addressing the uncertainties in satellite-derived estimates and improving the reliability of NPP predictions, our work contributes to advancing the field of marine remote sensing and provides a foundation for future research.

An important limitation of this study is that the probabilistic prediction models were trained on outputs from existing NPP models rather than directly on observational data. This introduces the potential for inherited biases and errors from the base models, limiting the generalizability of our uncertainty estimates to true NPP values. Future research should prioritize incorporating in situ NPP measurements to refine model training and validation, enabling more accurate and reliable uncertainty quantification.

830 The differences between VGPM, CbPM, and CAFE outputs underscore the challenges

831 in determining the most reliable NPP training data. While CAFE was chosen as the

832 primary prediction target, this choice was informed by prior studies highlighting its

833 strengths in parameterizing key oceanic processes and by the strong predictive

834 performance of the NN and Bayesian models when using CAFE outputs. We

835 acknowledge that this approach inherits the limitations of the base models and that

836 further validation with in situ measurements is necessary to ensure that CAFE outputs

837 align closely with true NPP values. While our approach demonstrates strong potential

838 for accurately quantifying NPP uncertainty in this specific marine area, its application

839 to larger regions may encounter scalability challenges. This limitation arises due to the

840 large number of input variables required for the neural network and Bayesian

841 probabilistic models, which necessitate significant computational resources and

842 extensive observational data coverage.

843 In the context of ongoing climate change, accurately capturing and reducing the

844 uncertainty of marine NPP emerges as a key research focus in marine ecology. This

845 endeavor is crucial for a deeper understanding of energy and matter flow in marine

846 ecosystems, providing a solid scientific foundation for the judicious management of the

847 conservation of natural resources. While our study has advanced the field by

848 demonstrating the feasibility of probabilistic prediction in quantifying NPP uncertainty,

849 we acknowledge the potential for further enhancements and expansions. Looking ahead,

850 future research could embark on the following paths to augment our work: (1)

851 Expanding the research scope: The current study has concentrated primarily on specific

852 marine areas. Future initiatives could broaden this focus to encompass diverse

853 geographic regions and types of marine ecosystems. However, such an expansion

854 would require addressing the scalability limitations inherent to the current models, such

855 as their reliance on a high volume of input variables and computational resources.

856 Investigating strategies to simplify model inputs or develop hierarchical approaches

857 that adapt to varying data availability and resolution across broader regions would be

858 critical for enhancing scalability. This expansion is vital to gain a more comprehensive

understanding of probabilistic prediction's applicability and effectiveness across varying environmental conditions; (2) Enhancing data collection~~: The acquisition of more extensive~~ and utilization: Access to a wider and more comprehensive ~~observational data is instrumental in refining~~set of observations can help refine model training and improve prediction accuracy~~. Future endeavors should aim to amass a richer array of observational data, emphasizing the need for long-term time series and high-resolution remote sensing data. These~~, and in addition, efforts to analyze the importance of features on data variables and to eliminate redundant features to reduce the input of extraneous variables will ~~significantly bolster~~greatly facilitate the development and validation of robust probabilistic prediction models; (3) Refining model structure: Our study utilized Bayesian probabilistic regression and deep learning-based probabilistic prediction models. Future studies could explore the integration of other advanced model structures or the optimization of the existing ones, aiming to elevate the model's performance and robustness. Through these concerted efforts, we aspire to continually refine the methodologies of probabilistic prediction in quantifying marine NPP uncertainty, thereby laying the groundwork for more precise ecosystem management and environmental protection strategies.

Author contribution Statement

Jie Niu: Conceptualization, Methodology, Data Curation, Writing - Review & Editing, Supervision, Funding acquisition.

Mengyu Xie: Conceptualization, Methodology, Data Curation, Writing - Original Draft, Visualization.

Yanqun Lu: Conceptualization, Methodology, Data Curation, Writing - Original Draft, Visualization.

Liwei Sun:Data Curation, Supervision,Funding acquisition.

Na Liu: Writing - Review & Editing, Supervision.

Han Qiu: Writing - Review & Editing, Supervision.

Dongdong Liu: Writing - Review & Editing, Supervision.

887 Chuanhao Wu: Writing - Review & Editing, Supervision.

888 Pan Wu: Writing - Review & Editing, Supervision.

Declaration of interests

890 The authors declare that they have no known competing financial interests or personal
891 relationships that could have appeared to influence the work reported in this paper.

Acknowledgements

893 This research was funded by the National Natural Science Foundation of China
894 [41972244], the Project of Science and Technology Department of Guizhou Province
895 (the technical system of prevention and control to mine groundwater pollution in karst
896 areas, 2022), ~~and~~ the High-Level Talent Training Program in Guizhou Province
897 (GCC[2023]045), and Guizhou Provincial Qiankehe Talent Program (KJZY[2025]
898 030). Co-author Liwei Sun was partially supported by GuangDong Basic and Applied
899 Basic Research Foundation (2022A1515010590).

References

901 Al-Gabalawy, M., Hosny, N. S., & Adly, A. R. (2021). Probabilistic forecasting for energy time series
902 considering uncertainties based on deep learning algorithms. Electric Power Systems Research, 196,
903 107216.

904 Behrenfeld, M. J., & Falkowski, P. G. (1997). Photosynthetic rates derived from satellite-based
905 chlorophyll concentration. Limnology and oceanography, 42(1), 1-20.

906 Behrenfeld, M. J., Boss, E., Siegel, D. A., & Shea, D. M. (2005). Carbon-based ocean productivity and
907 phytoplankton physiology from space. Global biogeochemical cycles, 19(1).

908 Braarud T. Salinity as an ecological factor in marine phytoplankton[J]. Physiologia Plantarum, 1951,
909 4(1).

910 BIPM, I., IFCC, I., ISO, I., & IUPAP, O. (2009). Evaluation of measurement data– an introduction to the
911 'Guide to the expression of uncertainty in measurement' and related documents. JCGM, 104, 1-104.

912 Cael, B. B. (2021). Variability-based constraint on ocean primary production models. Limnology and
913 Oceanography Letters, 6(5), 262-269.

914 Campbell, J., Antoine, D., Armstrong, R., Arrigo, K., Balch, W., Barber, R., ... & Yoder, J. (2002).
915 Comparison of algorithms for estimating ocean primary production from surface chlorophyll,
916 temperature, and irradiance. Global biogeochemical cycles, 16(3), 9-1.

917 Dave, A. C., & Lozier, M. S. (2013). Examining the global record of interannual variability in
918 stratification and marine productivity in the low-latitude and mid-latitude ocean. Journal of
919 Geophysical Research: Oceans, 118(6), 3114-3127.

920 Ding, Q. X., Chen, W. Z. (2016). Spatial and Temporal Variations in Net Primary Productivity in the
921 China Seas Based on VGPM. Marine Development and Management, 8, 31-35.

922 Dürr, O., Sick, B., & Murina, E. (2020). Probabilistic deep learning: With python, keras and tensorflow
923 probability. Manning Publications.

924 Falkowski, P. G., Barber, R. T., Smetacek, V. (1998). Biogeochemical Controls and Feedbacks on Ocean
925   Primary Production. Chemistry and biology of the oceans, 281, 200-206

926 Gneiting, T., & Katzfuss, M. (2014). Probabilistic forecasting. Annual Review of Statistics and Its
927   Application, 1, 125-151.

928 Guan, W., He, X., Pan, D., Gong, F. (2005). Remote sensing estimation of primary productivity in the
929   Bohai Sea, Yellow Sea, and East China Sea. Journal of Fisheries of China, 29(3), 367-372.

930 Hersbach, H. (2000). Decomposition of the continuous ranked probability score for ensemble prediction
931   systems. Weather and Forecasting, 15(5), 559-570.

932 He J., Huang Z. (2019). The distribution of corals in weizhou island, guangxi. Ocean Dev. Manage. 1,
933   57‐62.

934 Juban, J., Siebert, N., & Kariniotakis, G. N. (2007). Probabilistic short-term wind power forecasting for
935   the optimal management of wind generation. In 2007 IEEE Lausanne Power Tech (pp. 683-688).
936   IEEE.

937 Kaplan D. (2021). On the Quantification of Model Uncertainty: A Bayesian Perspective. Psychometrika,
938   86(1):215-238.

939 Lee, Z., Marra, J., Perry, M. J., Kahru, M. (2015). Estimating Oceanic Primary Productivity from Ocean
940   Color Remote Sensing: A Strategic Assessment. Journal of Marine Systems, 149, 50–59.

941 Li, W., Tiwari, S. P., El-Askary, H. M., Qurban, et al. (2020). Synergistic use of remote sensing and
942   modeling for estimating net primary productivity in the red Sea with VGPM, eppley-VGPM, and
943   CbPM models intercomparison. IEEE Transactions on Geoscience and Remote Sensing, 58(12),
944   8717-8734.

945 Li C., Wang F. (2004). Holocene volcanic effusion in Weizhou Island and its geological significance.
946   Miner. Petrol 4, 28‐34.

947 Matheson, J. E., & Winkler, R. L. (1976). Scoring rules for continuous probability
948   distributions. Management science, 22(10), 1087-1096.

949 Milutinović, S., & Bertino, L. (2011). Assessment and propagation of uncertainties in input terms through
950   an ocean-color-based model of primary productivity. Remote Sensing of Environment, 115(8),
951   1906-1917.

952 Pan, X., Wong, G. T., Shiah, F. K., & Ho, T. Y. (2012). Enhancement of biological productivity by internal
953   waves: observations in the summertime in the northern South China Sea. Journal of
954   oceanography, 68, 427-437.

955 Pic, R., Dombry, C., Naveau, P., & Taillardat, M. (2023). Distributional regression and its evaluation
956   with the CRPS: Bounds and convergence of the minimax risk. International Journal of
957   Forecasting, 39(4), 1564-1572.

958 Platt, T., & Sathyendranath, S. (1988). Oceanic primary production: estimation by remote sensing at local
959   and regional scales. Science, 241(4873), 1613-1620.

960 Platt, T., Caverhill, C., & Sathyendranath, S. (1991). Basin-scale estimates of oceanic primary production
961   by remote sensing: The North Atlantic. Journal of Geophysical Research: Oceans, 96(C8), 15147-
962   15159.

963 Ryther, J. H. (1956). Photosynthesis in the Ocean as a Function of Light Intensity 1. Limnology and
964   Oceanography, 1(1), 61-70.

965 Ryther, J. H., & Yentsch, C. S. (1957). The estimation of phytoplankton production in the ocean from
966   chlorophyll and light data 1. Limnology and oceanography, 2(3), 281-286.

967 Saba, V. S., Friedrichs, M. A., Antoine, D., Armstrong, R. A., Asanuma, I., Behrenfeld, M. J., ... &
968   Westberry, T. K. (2011). An evaluation of ocean color model estimates of marine primary
969   productivity in coastal and pelagic regions across the globe. Biogeosciences, 8(2), 489-503.

970 Sathyendranath, S., Longhurst, A., Caverhill, C. M., & Platt, T. (1995). Regionally and seasonally
971   differentiated primary production in the North Atlantic. Deep Sea Research Part I: Oceanographic
972   Research Papers, 42(10), 1773-1802.

973 Sathyendranath S., Platt T., Kovač Ž., et al. (2020). Reconciling models of primary production and
974   photoacclimation. Applied Optics, 59(10):C100-C114.

975 Schepen, A., Zhao, T., Wang, Q. J., & Robertson, D. E. (2018). A Bayesian modelling method for post-
976   processing daily sub-seasonal to seasonal rainfall forecasts from global climate models and
977   evaluation for 12 Australian catchments. Hydrology and Earth System Sciences, 22(2), 1615-1628.

978 Schwanenberg, D., Fan, F. M., Naumann, S., Kuwajima, J. I., Montero, R. A., & Assis dos Reis, A. (2015).
979   Short-term reservoir optimization for flood mitigation under meteorological and hydrological
980   forecast uncertainty. Water Resources Management, 29(5), 1635-1651.

981 Silsbe, G. M., M. J. Behrenfeld, K. H. Halsey, A. J. Milligan, and T. K. Westberry. (2016), The CAFE
982   model: A net production model for global ocean phytoplankton, Global Biogeochem. Cycles, 30,
983   1756–1777, doi:10.1002/2016GB005521.

984 Tan, S. C., Shi, G. Y. (2005). Satellite Remote Sensing of Marine Primary Productivity. Advances in
985   Earth Science. ~~Advances in Earth Science~~Advances in Earth Science, 20(8).

986 Tan, S. C., Shi, G. Y. (2006). Remote sensing study on the primary productivity and its spatiotemporal
987   variation in the Chinese coastal seas. Acta Geographica Sinica, 61(11), 1189-1199.

988 Westberry, T. K., Silsbe, G. M., & Behrenfeld, M. J. (2023). Gross and net primary production in the
989   global ocean: An ocean color remote sensing perspective. Earth-Science Reviews, 104322.

990 Perfors A, Tenenbaum J B, Griffiths T L, et al. A tutorial introduction to Bayesian models of cognitive
991   development[J]. Cognition, 2011, 120(3): 302-321.

992 Westberry, T., Behrenfeld, M. J., Siegel, D. A., & Boss, E. (2008). Carbon-based primary productivity
993   modeling with vertically resolved photoacclimation. Global Biogeochemical Cycles, 22(2).

994 Westberry, T., Behrenfeld, M. J., Siegel, D. A., Boss, E. (2008). Carbon-based primary productivity
995   modeling with vertically resolved photoacclimation. Global Biogeochemical Cycles, 22(2).

996 Yang, B. (2021). Seasonal relationship between net primary and net community production in the
997   subtropical gyres: Insights from satellite and Argo profiling float measurements. Geophysical
998   Research Letters, 48(17), e2021GL093837.

999 Yu W., Wang W., Yu K., Wang Y., Huang X., Huang R., et al. (2019). Rapid decline of a relatively high
1000   latitude coral assemblage at weizhou island, northern south China Sea. Biodivers. Conserv. 28 (14),
1001   3925–3949.

1002 Yang, B., Fox, J., Behrenfeld, M. J., Boss, E. S., Haëntjens, N., Halsey, K. H., et al. (2021). In situ
1003   estimates of net primary production in the western North Atlantic with Argo profiling floats. Journal
1004   of Geophysical Research: Biogeosciences, 126, e2020JG006116.

1005 Zamo, M., & Naveau, P. (2018). Estimation of the continuous ranked probability score with limited
1006   information and applications to ensemble weather forecasts. Mathematical Geosciences, 50(2), 209-
1007   234.

1008 Zhao, T., Wang, Q. J., Bennett, J. C., Robertson, D. E., Shao, Q., & Zhao, J. (2015). Quantifying
1009   predictive uncertainty of streamflow forecasts based on a Bayesian joint probability model. Journal
1010   of Hydrology, 528, 329-340.

1011 Zhao, T., Wang, Q. J., Bennett, J. C., Robertson, D. E., Shao, Q., & Zhao, J. (2015). Quantifying
1012   predictive uncertainty of streamflow forecasts based on a Bayesian joint probability model. Journal
1013   of Hydrology, 528, 329-340.

1014 Zou, Q., & Wen, J. (2024). Battery state-of-health estimation incorporating model uncertainty based on
1015   Bayesian model averaging. Energy, 308, 132884.

1016

1017 **Tables**

1018 **Table 1.** Summary of Variables and Data Sources.

Variable name	Variable description	Data source
SST	Sea surface temperature (°C)	
Sal	Salinity (‰)	
TH	Height of tide(m)	
AP	Air pressure (hPa)	Weizhou Marine environment
RH	Relative humidity (%)	monitoring station
SV	Sea visibility (km)	
WS	Wind speed (m·s^{-1})	
H/10	1/10th significant wave height (m)	
PAR	Photosynthetically active radiation (W·m^{-2})	Oceancolor
SSP	Sea surface precipitation (mm)	Earthdata
SH	Sunshine hours (h·d^{-1})	China Meteorological Administration
VGPM	NPP from the VGPM model (mgC m^{-2}·d^{-1})	
CbPM	NPP from the CbPM model (mgC m^{-2}·d^{-1})	Ocean Productivity
CAFE	NPP from the CAFE model (mgC m^{-2}·d^{-1})	

1019 **Table 2.** Summary of Missing Variables.

Variable	SV (km)	H/10 (m)	PAR (W·m^{-2})	SSP (mm)	SH (h·d^{-1})
Missing quantity (days)	31	51	828	378	18

1020 **Table 3.** Statistics of data pre- and post-interpolation.

	SV (km)		H/10 (m)		PAR (W·m^{-2})		SSP (mm)		SH (h·d^{-1})	
	pre-	post-	pre-	post-	pre-	post-	pre-	post-	pre-	post-
count	4046	4077	4026	4077	3249	4077	3699	4077	4059	4077
mean	15.22	15.23	0.57	0.57	34.92	35.97	4.94	4.85	5.19	5.18
std	10.33	10.30	0.41	0.41	15.64	15.20	16.13	15.61	3.93	3.93

min	0.00	0.00	0.00	0.00	1.20	1.20	0.00	0.00	0.00	0.00
25%	7.00	7.00	0.30	0.30	22.19	24.14	0.00	0.00	0.80	0.80
50%	12.00	12.00	0.50	0.50	36.03	36.87	0.00	0.00	5.60	5.60
75%	25.00	25.00	0.70	0.70	47.58	48.49	1.30	1.50	8.90	8.80
max	50.00	50.00	4.00	4.00	61.13	61.13	280.40	280.40	12.6	12.6

Table 4. Parameters of the Neural Network Model

	Hyper-parameters	
Layer Sizes	Layer 1	64
	Layer 2	32
	Layer 3	16
	Layer4	16
	Layer 5	2
	Distribution Layer	Gaussian distribution
Epochs	800	
Learning Rate	0.0001	
Batch Size	16	
optimizer	Adam	
loss	Negative log likelihood	

Table 5. CRPS, RMSD, MAPD, and proportion of input data within 95% confidence interval.

	CRPS		RMSD		MAPD		Proportion	
	Train	Test	Train	Test	Train	Test	Train	Test
NN	0.096	0.133	0.149	0.198	11.828	13.237	0.971	0.932
Bayes	0.151	0.20	0.201	0.253	13.909	14.145	0.976	0.951
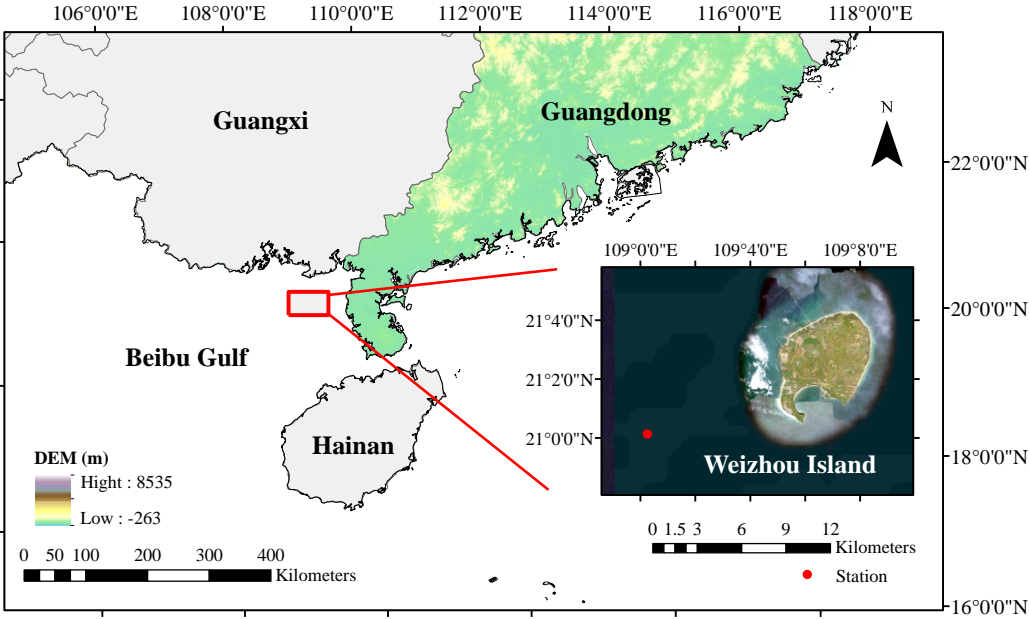
Figures

Fig. 1. The research area is located in the waters of Weizhou Island in Beibu Gulf, south China. The red dots in the figure indicate the location of Weizhou Marine Environmental Monitoring Station (21.0017°N, 109.0117°E). Eight distinct sets of monitoring data were collected from this monitoring station.

1031
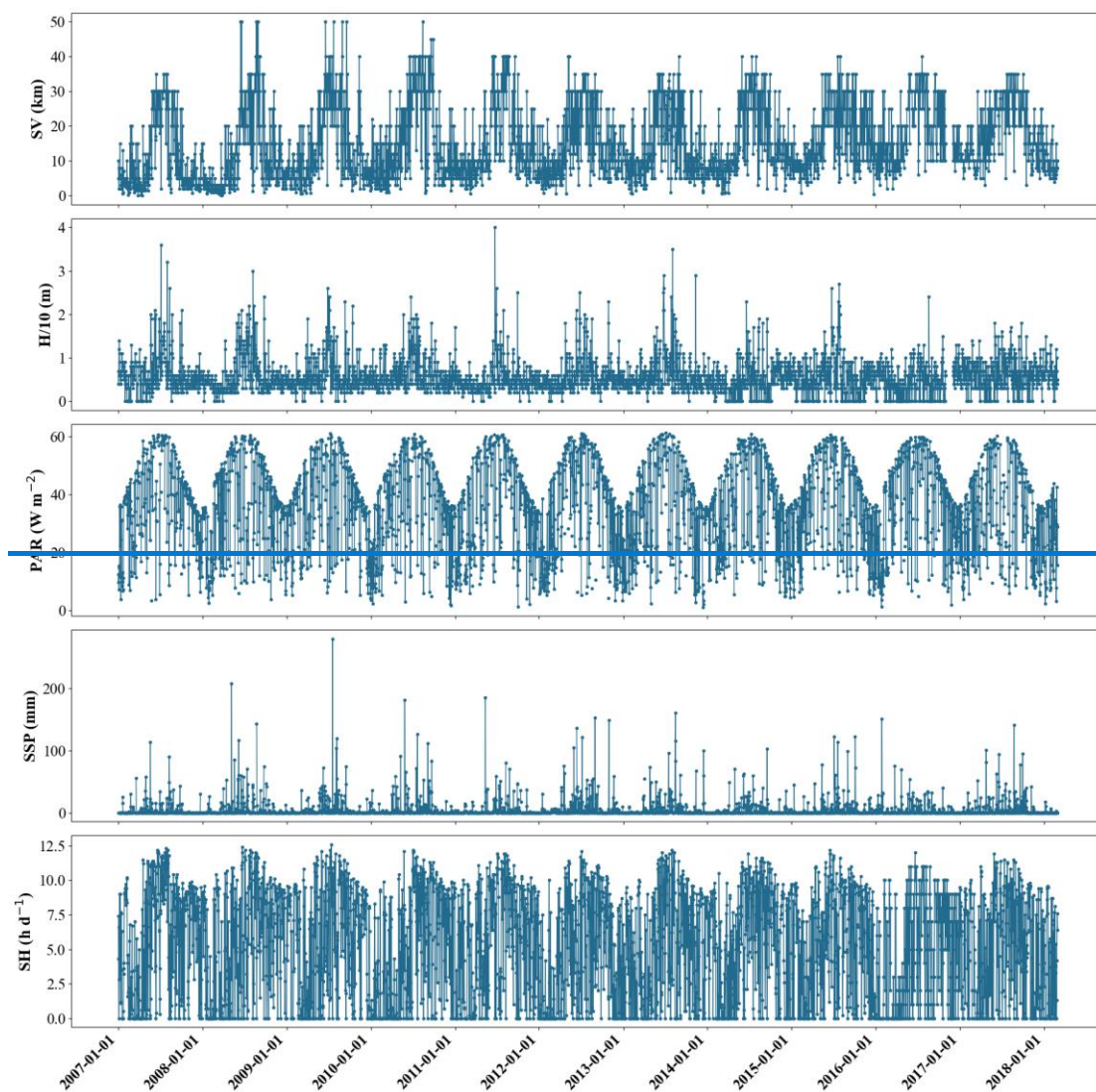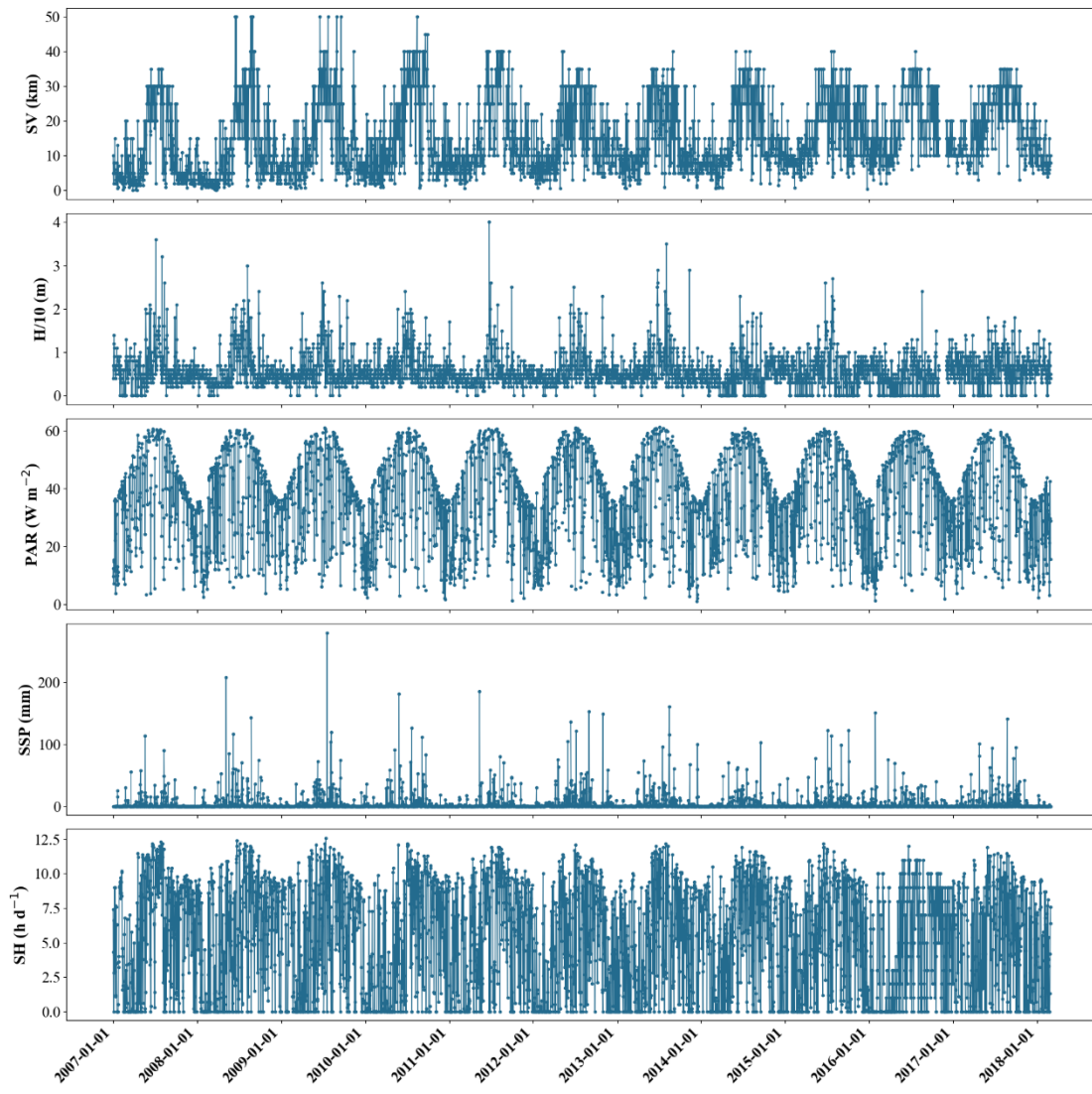
Fig. 2. Time series plots of SV, H/10, PAR, SSP, and SH with missing variables, showing the
cyclical variation of these five variables.

1034
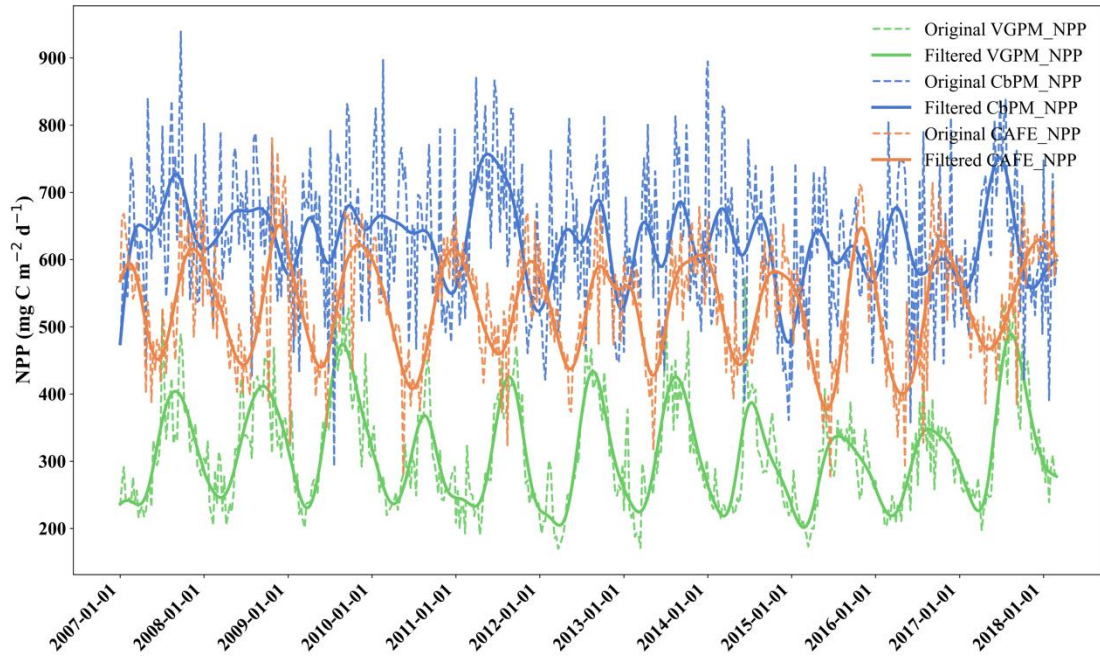
Fig. 3. Time series of VGPM, CbPM, and CAFE from January 2007 to February 2018, where the green line represents VGPM, the blue line represents CbPM, and the orange line represents CAFE-. The dashed lines are the original data and the solid ones are the low-pass filtered, which show the seasonal variations more clearly. Abbreviations and data sources can be referenced in Table 1.

1040
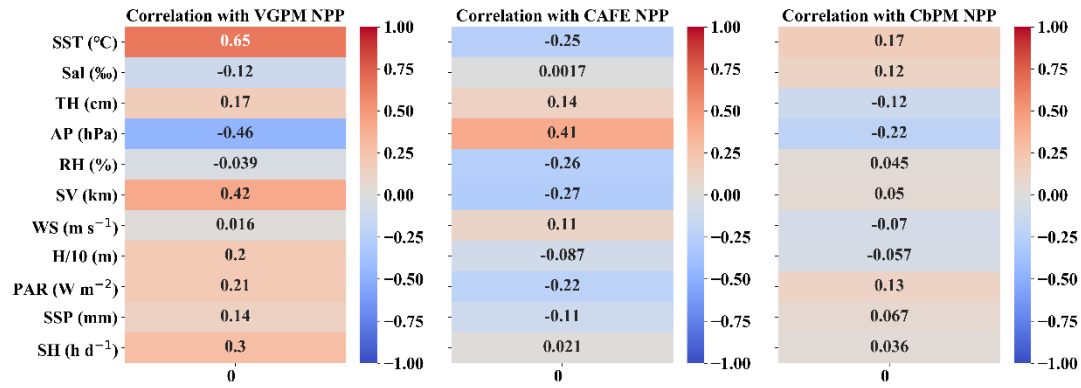
Fig. 4. Pearson correlation between the 11 input variables and the three NPPs (VGPM, CAFE, and CbPM). These input variables serve as inputs to the probabilistic models, while VGPM, CAFE, and CbPM are used as model outputs. The deeper the shade of red indicates a stronger positive correlation, whereas the deeper shade of blue indicates a stronger negative correlation.

1045
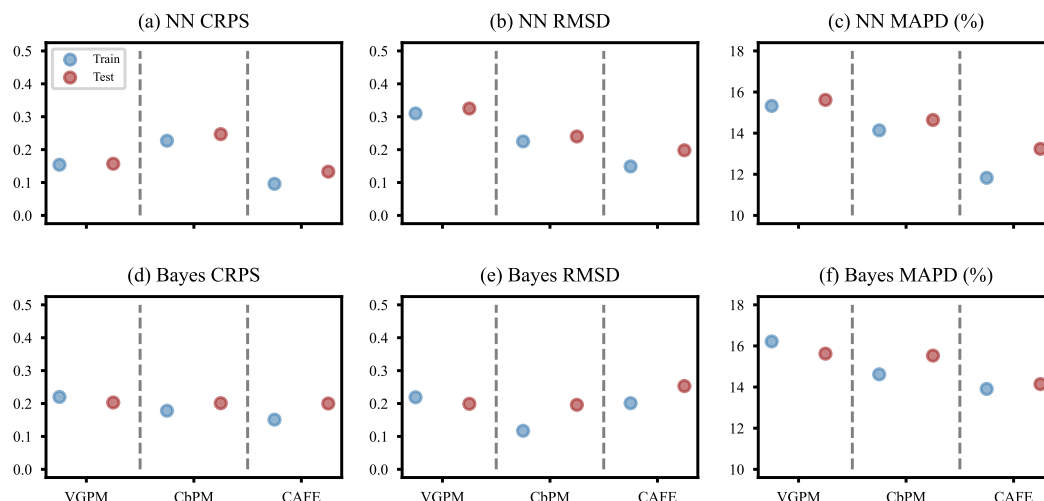
Fig. 5. Comparison of NPP predictive effects from VGPM, CbPM, and CAFE. Panels (a)–(c) present the results from the neural network-based probabilistic prediction models; panels (d)–(f) the results from Bayesian probabilistic prediction models based on empirical distributions. The horizontal coordinates represent the VGPM, CbPM, CAFE as inputs in sequence, separated by gray dashed lines, where blue dots represent data from the training set, and red dots denote data from the test set, and the vertical coordinates are the values of the three metrics, CRPS, RMSD, MAPD. Since NPP values were normalized to the range of $0-1$, the y axes of subplots (a), (b), (d), and (e) are dimensionless. The units for MAPD are percentile.

1054
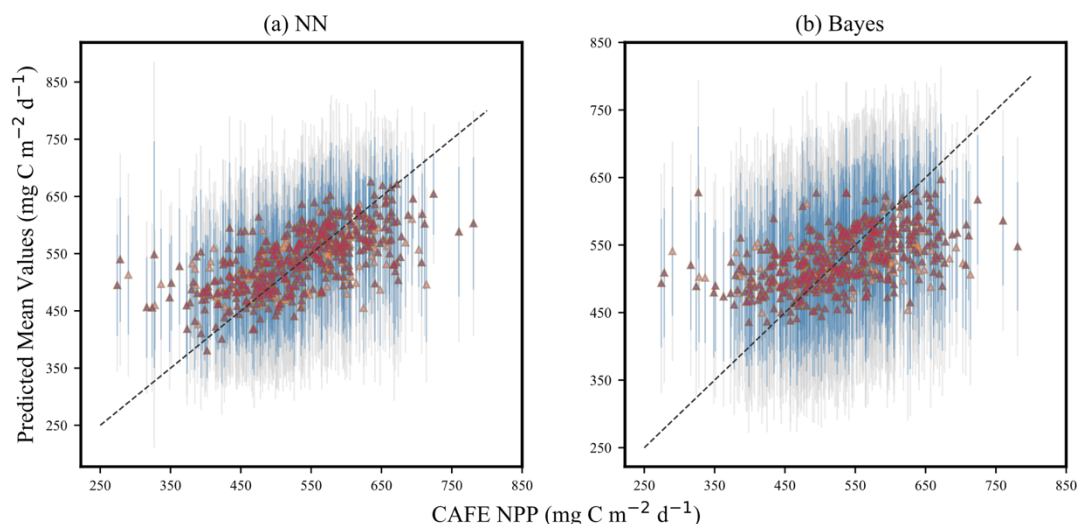
Fig. 6. Uncertainty quantification of (a) neural network-based probabilistic prediction model and (b) empirical distribution-based Bayesian probabilistic prediction model. The horizontal axes represent the input CAFE value, while the vertical axes show the mean predicted by the model. The triangular icons in the figure represent 514 sets of the forecast average, the gray vertical lines represent the 95% confidence intervals for the predictions, and the blue vertical lines represent the 75% confidence intervals.

1061
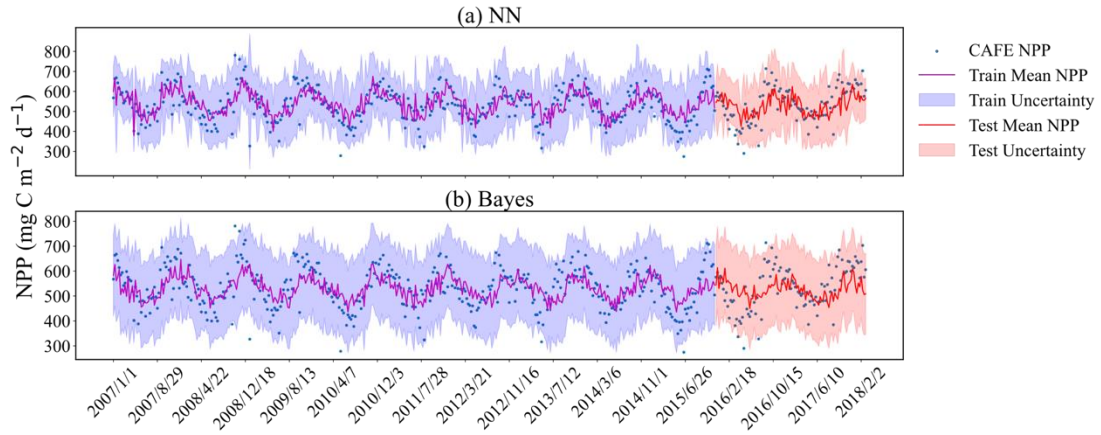
Fig. 7. Comparison of original and predicted mean values shown at an 8-day temporal resolution within a 95% confidence interval. (a) Probabilistic prediction results based on neural networks; (b) Bayesian probabilistic prediction results based on empirical distributions. The dashed lines represent the mean values of the probabilistic predictions. The purple and red shaded areas illustrate the uncertainty ranges for the training and the test sets, respectively. Blue dots signify observed data points. All predictions and observations are presented in chronological sequence.

1068
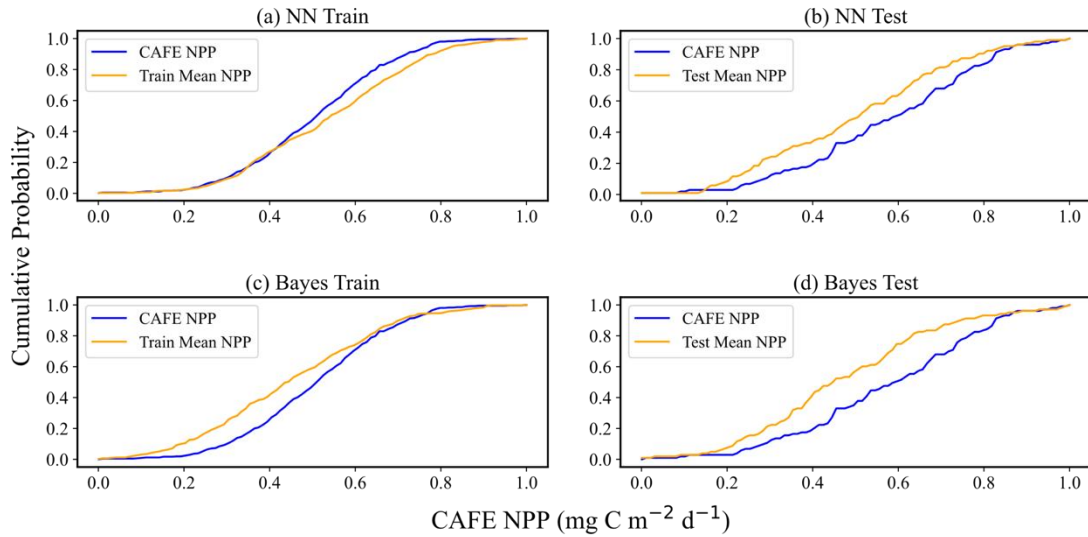
Fig. 8. Comparison of CAFE and predicted mean CDF. Panels (a) and (b) display the performance of the training and test sets, respectively, in the neural network-based probabilistic prediction model. Panels (c) and (d) illustrate the performance of the training and test sets, respectively, in the empirical distribution-based Bayesian probabilistic prediction model. The data has been normalized to a scale of 0–1 to ensure consistency across metrics and facilitate direct comparison between the two models. In each panel, the blue curves represent the CDFs of the CAFE values, while the yellow curves depict the CDFs of the model's predicted mean values.

1076
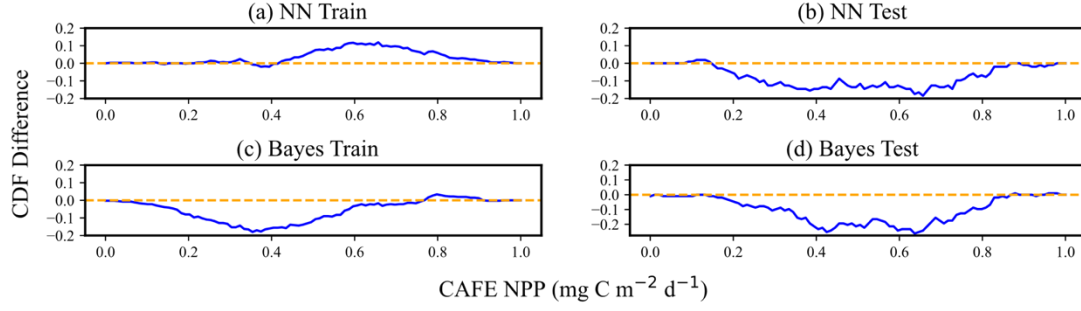
Fig. 9. Difference between the CAFE CDF and predicted mean CDF of model predictions. Panels (a) and (b) represent the performance of the training set and test sets, respectively, in the neural network-based probabilistic prediction model. Panels (c) and (d) showcase the performances of the training set and test sets, respectively, in the empirical distribution-based Bayesian probabilistic prediction model. The residuals are expressed in normalized units (0–1), enabling consistent assessment of model performance across different NPP ranges. The blue curves in each panel indicate the differential magnitude of the CDFs. Instances where the blue curves align with the yellow lines denote zero discrepancy between the input data CDF and the model's predicted mean CDF.

1086
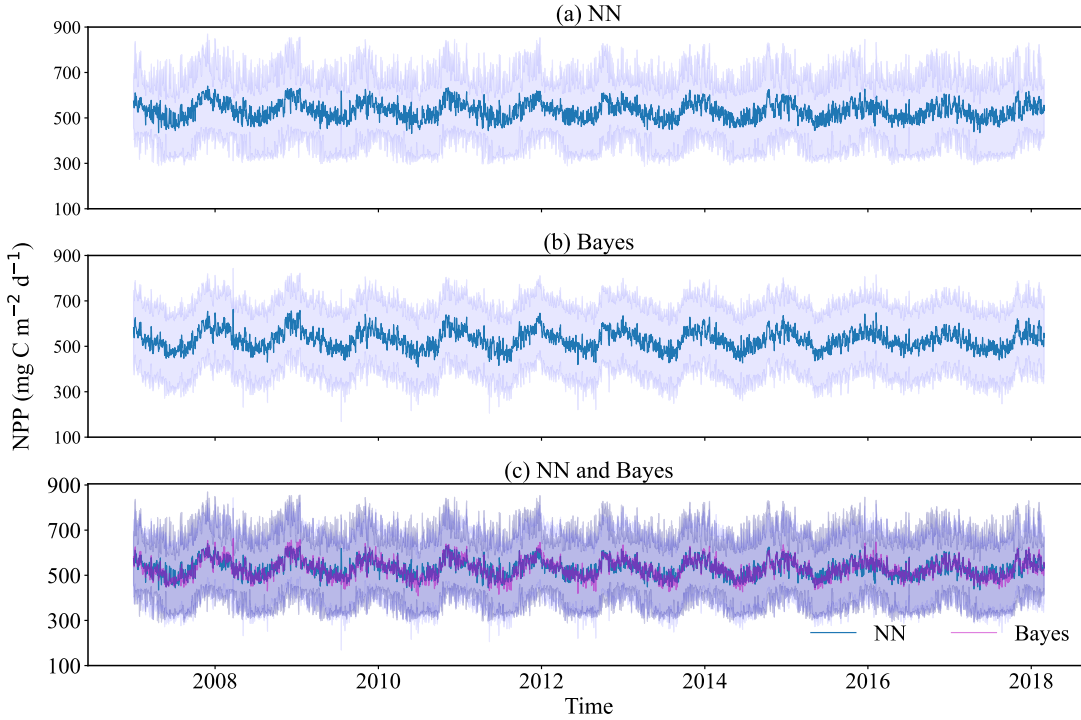
Fig. 10. Time series plots of daily probabilistic NPP predictions in Weizhou Island (2007 – March 2018). (a) Probability prediction results of the neural network model; (b) Bayesian probability prediction results based on empirical distribution; (c) Comparison of the two models' predictions, with the green lines representing the mean predictions from the neural network model and the gray lines depicting the mean predictions from the Bayesian model.

1092
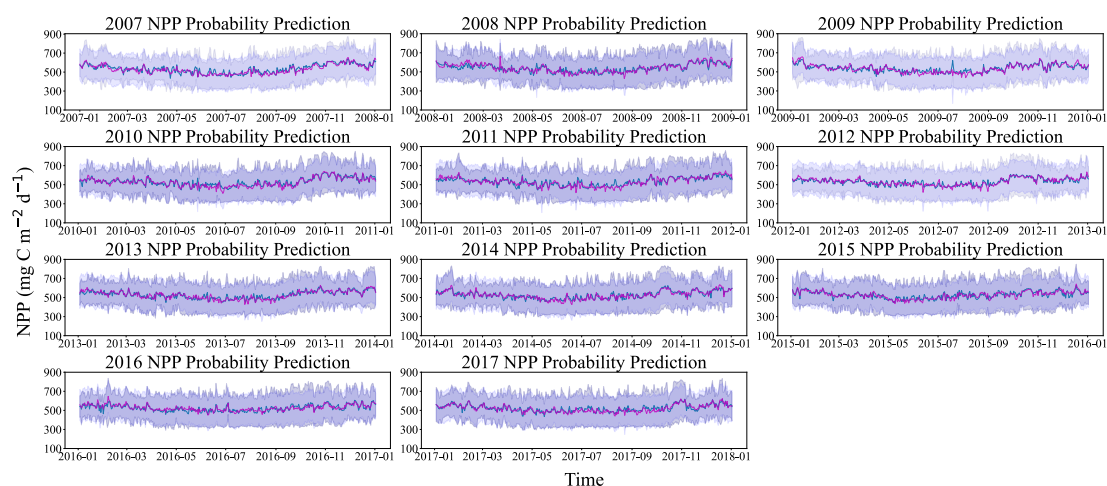
Fig. 11. Time series plots of probabilistic NPP predictions in Weizhou Island (2007 – 2017). The
light purple shading indicates the 95% confidence interval of the Bayesian model, while the dark
purple shading represents the 95% confidence interval of the neural network model. The green lines
show the mean prediction values from the neural network model; and the gray lines depict the mean
prediction values from the Bayesian model.